JOINT EUROPEAN TORUS JET

JET–P(93)28

R.D. Gill

Generation and Loss of Runaway Electrons following Disruptions in JET

Generation and Loss of Runaway Electrons following Disruptions in JET

R.D. Gill

JET-Joint Undertaking, Culham Science Centre, OX14 3DB, Abingdon, UK

Preprint of a paper to be submitted for publication in
Nuclear Fusion
April l993

ABSTRACT

Detailed observations are presented on the generation and loss of runaway electrons following density limit disruptions in the JET tokamak with carbon limited discharges. Direct observations are made of the runaways from detection of the high energy bremsstrahlung radiation from the runaway - background plasma interactions. The different stages of the disruption leading to the runaway production are identified. It is shown that control of the current channel is important in preventing damaging interactions between the runaways and the vessel walls.

1. INTRODUCTION

The generation and loss of runaway electrons following disruptions have potentially serious consequences in large tokamaks if the electrons are dumped into the limiter or vessel walls. In JET, the generation of large runaway currents in carbon limited discharges has been regularly observed[1]) and studies have been made[2]) of the subsequent neutron production from (γ,n) reactions. A fairly systematic study[3]) of these disruptions has been made for discharges with both C and Be limiters. This has shown that runaway generation occurs principally in C limited discharges, with reduced runaways in X-point configurations, and few in Be limited discharges of any configuration. This paper will present detailed observations and interpretations on the production and loss of the runaways in C limited discharges.

Generally the effects of runaways have been observed when they strike the torus walls and produce showers of gamma rays, and neutrons. The activation of the wall by this process has been routinely observed in many tokamaks[4]). In some tokamaks, measurements of the direct synchrotron radiation also exist for discharges which contain runaways in the plasma flat-top[5]). In this paper direct observations made of the runaways electrons within the torus are presented. These measurements are due to the very high energy bremsstrahlung radiation emitted by the runaways in collisions with the background plasma ions and are a new way of studying the runaways.

Nearly all the observations reported in this paper have been made with a Si diode camera arrays, with hard X-rays observed by detectors blanked off from the

plasma by thick metal plates. The details of the systems are given in Appendix 1 and their locations on the machine are shown in fig. 1.

2. RUNAWAY PRODUCTION

Plasma disruptions are complicated phenomena generally preceded by a large variety of mhd phenomena[1]). In the case of density limit disruptions the first precursor to a disruption is often a large increase in the plasma radiated power (P_{rad}) to a value greater than the input power (P_{in}). This leads to plasma contraction and detachment from the limiter with the development of marfes[3]). Growth of mhd modes follows, generally m=2, but occasionally m=3 also, and in JET these modes generally lock when they become of large amplitude. Minor disruptions are a general feature of this stage, but these often have relatively small effects on the plasma current and the loop volts. The minor disruptions cause considerable changes in plasma profiles, with a general flattening of the central pressure. The major disruption is always preceded by one or two ms by a profile erosion which is probably due to the interaction of many modes[6]). It has been proposed[7]) that this erosion *is* the major disruption even though the effects on the current and voltage do not become apparent until a few ms later when the large negative voltage spike and changes to the plasma current are seen.

Other disruptions at low q or high current[8]) have different behaviour prior to the erosion and the negative voltage spike, and many disruptions are found at high current which are not preceded by $P_{rad} \geq P_{in}$. In these disruptions, m=n=1 perturbations play an important role and it was found that there was a limiting internal inductance which, when reached, produced a plasma which would probably disrupt.

The processes preceding the major disruption have been presented in refs.[1,8]); here the main interest is in the processes which occur during the major disruption itself, which lead to the runaway production. These are illustrated in fig. 2 where traces of the soft and hard X-rays, the loop volts and plasma current are shown. The period preceding stage I is the predisruptive phase which contains the varied mhd activity and mode growth and locking, the radiation domination, marfes and other phenomena closely related to disruption precursors. The major disruption itself is preceded by stage I, where an unusual and characteristic profile erosion (fig. 3) is observed as has been previously reported[1]). This phenomena is closely related to the "cold bubbles" observed on

other machines[9,10]). The processes which occur during and after the major disruption leading to runaway production are summarised below.

2.1 Summary of processes leading to runaway production

Stage 1 All major disruptions are preceded by an event seen on the soft X-rays as a profile erosion which is probably due to the interactions of many modes.

Stage II After 1-2 ms the negative voltage spike is observed at the plasma edge and this is accompanied by a greatly increased soft X-ray emission, principally in the plasma edge regions. This is partly due to an increased plasma temperature in the edge region but is mainly due to a substantial increase in the plasma density and impurity concentration[11]).

Stage III As the impurity influx continues the plasma becomes cooled leading to a very rapid drop in T_e and soft X-ray emission, and a large increase in the loop volts. This marks the beginning of the generation of runaways. As T_e falls there is also evidence from the X-rays for a small (~15%) non-thermal component in the plasma with a temperature of about 15 keV.

Stage IV The bulk plasma becomes cold and the runaways build-up as can be seen from the hard X-ray signal. The runaway current makes a large contribution to the total current and causes a drop in the loop volts.

Stage V The runaways acquire MeV energies and are sometimes measured to be situated at small major radius well inside the original plasma centre. The loop volts drop to nearly zero and the runaway current becomes a substantial fraction of the original plasma current.

Either

Stage VIA If the control of the position of the runaways is inadequate then they are dumped onto the vessel walls and the current drops to zero. This is seen as large bursts of hard X-rays and is the moment at which

damage occurs to the vessel or limiters. This is the most probable sequence of events in JET.

or

Stage VIB The runaways are stabilised and the hard X-ray signal shows a smooth decay. A substantial plasma current remains for several seconds.

A more detailed description of each of these stages follows.

2.2 Detailed description of processes leading to runaway production

Stage I

All major disruptions are initiated by an event seen by the soft X-ray profiles as an erosion (Fig. 3). The erosion starts typically on one side of the profile at r/a = 0.3 and gradually spreads in ~ 1 ms to encompass a large volume of the plasma centre. An unusual feature is that the profile on the opposite side to the erosion seem largely unaffected by the process. An inversion radius is seen at large radius (r/a~ 0.5) outside of which increased X-ray emission is seen. Tomographic analysis of this erosion shows that it is not a simple mhd mode but looks rather like the invasion of the central region of the plasma with a cold bubble (fig. 4), as has also been subsequently observed on other machines,[9,10]).

The erosion is probably due to the interaction of many mhd modes and although it has an m=n=1 character the time dependence of the profiles shows that it is not a single mhd mode. This erosion leads to a flattening of the X-ray profile (and the pressure also). It has been suggested in ref.[7]) that the erosion *is* the disruption process and that substantial changes in the current take place at this time. Neither these nor the associated loop voltage changes are seen outside the plasma as the plasma in the edge regions is initially unaffected by the changes and can therefore act as a high conductivity screen with a long resistive time scale which prevents any electromagnetic disturbance from propagating outside the plasma. It would be desirable to check this supposed sequence of events by measuring the changes to the current distribution during this time.

Stage II

This is initiated when the loop volts start to drop, the plasma current increases and the soft X-ray emission increases rapidly, particularly at the plasma edge. A careful examination of the contour plot of the soft X-ray emission clearly shows that at this time the edge regions of the plasma start to emit X-radiation copiously on a rapid time scale. Before the stage II these regions of the plasma were far too cold to emit observable radiation and it therefore follows that mixing of the central plasma into the edge plasma must occur at this stage. The profiles of the X-ray emission rapidly become broader and flatter. However, the large overall increase in X-ray emission (fig. 5) cannot be understood simply by mixing and another mechanism must be involved. As the X-ray power, P_x, depends on $\Sigma n_e n_z f(T_e)$ either T_e must increase - for which there is no evidence - or the electron and/or impurity density must increase. A model based on this idea[11]) will give the necessary increase in P_x but it is not immediately obvious how the impurities can enter the plasma on the required time scale of ~100 μsec as diffusive time scales are far too long. The explosive neutral cloud model proposed in ref.[12]) may provide an explanation.

To illustrate the probable causes of the X-ray spike a model will be considered in which a plasma with an initial temperature, density and Z_{eff}, n_{eo} T_{eo} Z_{eo}, containing impurity ions of initial density n_{zo} and atomic number Z is subject to an inward impurity flux of the same impurity ions.

The X-ray power is

$$P_x = A\, n_e\, n_z f(T_e)$$

where A is a constant and with Be X-ray filters placed in front of the detectors $f(T_e) \propto T_e$. The electron energy content per unit volume is

$$W_e = \frac{3}{2} n_e\, k\, T_e$$

The impurity influx is given by

$$n_z = n_{zo}\,(1+\alpha t)$$

where α is a constant and

$$n_e = n_H + Z n_z$$

where n_H is the hydrogen density.

The energy balance will be affected by losses and gains from radiation, ohmic heating and diffusion. The influx of impurity ions will also cause a cooling on a rapid time scale due both to their ionisation and due to the introduction of cold electrons into the plasma which are subsequently heated to T_e. For influx of low Z ions both of these processes are sufficiently rapid to be of importance over the duration of the X-ray spike although the ionisation of the inner shells will be rather too slow. This will lead to an over estimate of calculated values of n_z.

Hence $$\frac{dW_e}{dt} = -\alpha Z \; n_{zo} E_i \; - P_r' + P_\Omega - P_c$$

where E_i is the mean ionization energy per electron and the terms on the right represent the energy required to ionise the impurity ions and heat the cold electrons, the radiation and conduction losses (P_r', P_c), and the ohmic heating (P_Ω). On rapid time scales all the terms except the first may be neglected. The radiated X-ray power is then

$$P_x = P_{xo} (1+\alpha t) (1-\alpha t/\beta)$$

where $\beta = W_{eo}/n_{zo} Z_i E_i$. β is large so that P_x initially increases, but later decreases in agreement with experiment.

A more detailed examination of the X-ray emission during the first spike reveals more complicated behaviour than predicted by the simple model. The temperature along a central chord may be determined on a rapid time scale by the two foil technique. The product of the density squared and the X-ray anomaly factor, ζ, is also determined. These show that the temperature remains approximately constant, but then falls rapidly to levels below 200 eV (the minimum determinable by this technique). $n_e^2\zeta$ rises steadily, doubling in 60 μsec. These observations give general support to the model even though the temperature does not decline as soon as would be expected. Towards the end of the spike the X-ray spectrum becomes non-thermal. A high energy tail appears which suggests that ~15% of the plasma electrons have an energy of ~ 16 keV. This could be the first stage of the runaway process.

Stage III

During this stage of the disruption the plasma becomes cold following the influx of impurities and the X-ray emission profiles are no longer smooth (fig. 5). A

very large loop volts develops which leads directly to the generation of the runaways. The physics of the runaway production has been discussed in many papers [13, 14, 15, 16]: the acceleration of the electrons occurs due to the imbalance between the friction force and the applied electric field, E. The ratio of E to the Dricer field, E_D, determines that runaways are generated if $E>E_D$ or equivalently, electrons will runaway if their velocity is greater than the critical velocity given by

$$v_c^2 = \frac{4\pi n_e e^3 \ell n\Lambda}{m_e E} = 7.8\text{x}10^3 \frac{n_e}{E}$$

For thermal plasmas in JET, values of v_c greater than the velocity of light are obtained and so few runaways can be produced. However, following the impurity influx and fall in T_e, E increases substantially due to the 100 fold increase in loop volts, reducing v_c so that runaways can then be generated. Typical values of $v_c = 6.7\text{x}10^9$ cm.s^{-1} are obtained corresponding to $T_e = 127$ eV. As this is much larger than the temperature of 25-50eV which would be inferred from the change in plasma resistivity it is clear that the plasma has entered a regime where strong runaway generation is possible. To calculate the fraction of the electrons which runaway with any degree of accuracy is difficult as it is an extremely sensitive function of the plasma parameters during the disruption and these are not well known. However, it is clear that the basic conditions for runaway generation are satisfied during this phase.

Calculations in ref. [15]) show the same behaviour as in observed: the loop volts increases rapidly and the current falls - both effects due to the very much reduced plasma conductivity. The electric field at the plasma centre is shown by the calculation to be very much higher than at the edge - perhaps up to 100 v.m^{-1} although the bulk of the runaway production was found to be produced nearer the edge in the lower density region. As the runaways begin to carry a large fraction of the current the loop volts start to fall eventually reaching a fraction of a volt. The calculations of Russo show that at this time the current is carried entirely by the electrons.

An estimate may be made of the runaway energy, assuming the runaways accelerate in free fall in an electric field, ξ. The equation of motion of the runaway electrons is

$$\frac{dp}{dt} = e\xi$$

If the experimentally measured valve of ξ is used then it is found that runaway energies of up to E_R = 35 MeV are obtained. This energy is achieved over 10-15ms and this time scale probably accounts for the slow rise seen in the hard X-ray signal (Fig. 2c). The hard X-ray signal also has a delayed onset after the loop volts start to rise substantially and this time delay is probably due to a threshold effect as it will be shown later that the efficiency of the hard X-ray detectors falls rapidly for energies below ~350 keV. The calculation shows that the time for the runaways to reach this energy is about 2 ms which is comparable to the observed delay in the hard X-ray signal. The time dependence of the runaway energy is shown in fig. 6 for acceleration in a uniform loop voltage of 100v.

It is thought that the hard X-ray signal originates either from runaway electrons which strike the vessel walls or from bremsstrahlung interactions between the runaways and the impurity ions in the torus. These both produce gamma rays at MeV energies. The runaways also lose energy by the synchrotron radiation at quanta energies well below the X-ray region. The efficiency for the hard X-ray detectors for gamma rays produced by relativistic electrons is calculated in Appendix B.

Stage IV

In the final stage the runaway electrons are, in some cases, situated at a small major radius with loop volts close to zero (fig. 7). The hard X-ray signal exhibits a smooth decay punctuated by prominent spikes (fig. 8). It is found that the smooth background, as measured in the set of detectors D is toroidally isotropic as it also is in detectors B (fig. 9), although at a lower intensity by a factor of 5.5. Further, the smooth background is seen only very weakly in the vertical camera whereas the spikes are quite strong. In contrast, the spikes are highly anisotropic (fig. 10) but the signals in both sets of detectors form a continuous distribution. The position of maximum emission varies from spike to spike. These facts support the idea that the smooth hard X-radiation is produced by bremsstrahlung interactions between the plasma and the background plasma. It will be shown later that the intensity difference between B and D is due to the highly anisotopic production of γ rays by relativistic electrons. The spikes are certainly due to loss of some of the relativistic electrons onto the vessel walls where they produce gamma radiation and neutrons as they slow down. The position of maximum emission of the spike then varies with the point of impact of the electrons. They have relative amplitude compared with the smooth background of ~2-8 and

have a duration of less than 300μs. The actual duration is probably determined by the characteristic slowing down time of ~ 30 MeV electrons in carbon limiters which is ~0.7 ns, well beyond our measurement capability.

3. CALCULATION OF OBSERVED HARD X-RAY SIGNAL IN RELATIVISTIC LIMIT

The observed hard X-ray signal from the bremsstrahlung may be calculated from the Heitler-Bethe cross-section, which, in the case of screening by the plasma for distances greater than λ_D, the Debye length, for relativistic electrons in a plasma[17]).

$$\sigma(E) = \frac{4Z^2 \alpha r_o^2 h}{E} \left\{ 1 + \left(\frac{p_f}{p_i} \right)^2 - \frac{2p_f}{3p_i} \right\} \ell n \left(\frac{2\lambda_D}{\alpha a_o} \right)$$

where p_i is the initial momentum and p_f, the final electron momentum, is $>> m_e c$. α is the fine structure constant, a_o the Bohr radius, and r_o the classical electron radius, h Planck's constant. The bremsstrahlung radiation is emitted into a forward cone within an angle $\theta \sim 1/\gamma = m_e c^2/E_R$. At high values of γ the electrons will emit their radiation in a narrow forward cone and for relativistic electrons moving in the median plane a small vertical band on the outside of the torus only will be illuminated. If the length of the horizontal port which can be illuminated in this way is ℓ then the fraction of the total power falling onto the plate is just $\ell/2\pi R_p$ where R_p is the major radius of the port.

Now the runaway current is $I_R = n_R e c \beta$ with $\beta = v/c$ and the actual number of runaways in the plasma is

$$2\pi R n_R = \frac{2\pi R I_R}{ec\beta}$$

The total radiated power deposited onto the port plate in the energy range dE_γ is

$$dP = \frac{\ell}{R_p} \frac{RI_R}{eh} n_z \sigma E \; dE$$

The results in the appendix show that the power in detector D may be related to the power deposited onto the port plate, P_F, by

$$P_x = 8.75 \times 10^{-10} P_F / (1 + E/3.2 \times 10^{-13})^2$$

where E is the gamma ray energy in ergs. Hence the power generated from X-rays in the energy range dE may be written as

$$dP_x = \frac{\ell R I_R n_z \sigma E \ dE}{R_p e h} \quad \frac{8.75x10^{-10}}{(1+E/3.2x10^{-13})^2}$$

where σ is the Heitler-Bethe cross-section. The total power may be found by integrating this expression from a cut off energy, E_c, to the energy of the electrons. An approximate value of P_x may be found when $E_R >> E_c$ given by

$$P_x = 1.19x10^{21} \frac{\ell R I_R n_z Z^2 \alpha r_o^2}{eR_p} \ell n\left(\frac{2\lambda}{a_o \alpha}\right)$$

which may be rewritten by introducing Z_{eff} as

$$P_x = 1.19x10^{21} \frac{\ell R I_R n_e Z_{eff} \ \alpha r_o^2}{eR_p} \ell n\left(\frac{2\lambda_D}{a_o \alpha}\right)$$

Evaluation of this expression with values ℓ=30, R=300, Z_{eff}=5, n_e=6x10^{13}, I_R=10^6, $\ell n \left(\frac{2\lambda_o}{a_o \alpha}\right)$=17, R_p = 400 gives $P_x \sim 7.0x10^{-7}$ W compared with measured values for a typical observation with 1MA of runaways of 5.4x10^{-7}W. This represents extremely good agreement and provides confirmation of the mechanism proposed. A similar calculation for detector B shows that the relative signals expected are in the ratio B:D of 1:4.5 which compares well with the observed ratio of 1:5.5.

An interesting feature of the expression for P_x is that it is proportional to $n_z Z_{eff} I_R$. As I_R is nearly constant in the post disruptive period, the fall in P_x must be due to a reduction of n_z and does not reflect the synchrotron loss time as has been previously thought[20]). The earlier conclusions were based on a much less exact representation of the efficiency of the detecting system which did not properly represent the data at low photon energies. This turns out to be very important due to the shape of the bremsstrahlung spectrum.

4. VARIABILITY OF BEHAVIOUR AND POSITION OF RUNAWAY CURRENT

There is a considerable variation in the behaviour of the plasma current and hard X-ray emission after the disruption as may be seen from Fig. 11. These differences seem to be closely related to the position control after the disruption. The position in major radius for the cases in Fig. 11 are shown in Fig. 12.

In some cases the plasma current channel is stabilised at small major radius, but in other cases the current channel moves inwards until it hits the inner wall. In these cases the runaways are generated while the plasma is moving and are dumped onto the walls at the same time as the current channel. In other cases, the position control system regains control of the plasma which then becomes centred within the vessel. In this case the runaways are not dumped onto the walls and the current decays gradually on a time scale of ~ 2 s. In this case the damaging effects of the runaways are avoided. The exact configuration of the runaway current after the disruption must be the subject of some speculation. The magnitude of this current is sufficient to generate a large poloidal field. The fact that the centre of the current distribution is sometimes quite close to the inner wall at major radius R (e.g. in discharge no. 11050 shown in fig. 7) suggests that the current must be carried in a tube with cross-sectional radius $(R-R_w)$ where R_w is the inner wall radius. The poloidal field produced at the surface of this tube would be 0.3T producing q=1.9. When the runaways are stabilised at the plasma centre (e.g. for discharge 13340) the q value is not constrained to such a low value. However, it is clear that the electrons in both cases move around the torus in helical orbits.

5. LOSS PROCESSES

It is generally assumed that once the runaways are established that they lose energy principally by synchrotron radiation due to their motion around the torus in an orbit with radius ≈ R. This is a very slow process with an energy loss time

of

$$\tau = 177\, R^2/\beta^3\gamma^3$$

which gives τ=73 sec for typical JET parameters. Because the runaway current depends on the velocity rather than the energy, the current decay time is very

much longer. This mechanism can clearly not account for the observed current decay times of about 1.9s.

Another possible effect which would reduce the runaway current is the small angle scattering of the runaway electrons on residual ions in the vessel. This has the effect of redirecting the runaways and thereby reducing the current flowing around the torus. The mean square scattering of a beam of relativistic electrons is given by

$$<\theta^2> \approx 2\pi N \left(\frac{2Ze^2}{pc}\right)^2 \ell n\Lambda \, c\tau$$

where N is the number of atoms per unit volume, Z their charge and $\ell n\,\Lambda$ is the Coulomb logarithm.

The plasma current may be written as

$$j = ne\, v_{11o} = ne\, v_{11o} <\cos\theta>$$

This current will be reduced by half by the scattering in a time

$$\tau = \frac{p^2c^2}{16\pi\, n_e Z_{eff}\, e^4\, c\, \ell n\, \Lambda}$$

where a summation has been carried out over the impurity species of the plasma.

There is considerable uncertainty about the density but the hard X-ray signal shows that this decays quite rapidly on a time scale of <<1 s to a value of less than $\frac{1}{10}$ of the post disruption value which the soft X-ray measurements suggest is two to three times the predisruption value. Using $n_e = 2\times10^{13}$ and plausible values for the other quantities gives τ~15 sec, again longer than the observed decay time of 2s.

An alternative explanation may be that the toroidal field ripple scatters the runaways as suggested by Laurent[17]) or that a small fraction of the runaways are continuously dumped on the vessel walls. It is difficult to imagine that this

would produce the very smooth hand X-ray signal seen in the discharges with a runaway current which persists for a very long period.

It should also be noted that when the electrons are scattered that they can lose their energy by synchrotron radiation very much more rapidly as the characteristic loss time may be written for electrons moving at an angle α to a parallel magnetic field as

$$\tau_{ES} = 3 \times 10^8/\gamma B^2 \beta^2 \sin^2\alpha$$

which for γ=70, B=27kG gives $\tau_{ES} = 5.87 \times 10^{-3}/\sin^2 \alpha$ which gives quite short times for very modest angles of scattering.

6. CONCLUSIONS

Detailed observations have been made of the hard X-radiation produced in discharges which have a large number of runaways following disruptions. The bremsstrahlung radiation due to runaway interactions with the residual plasma has been clearly observed at the expected intensity and this would offer a good way to diagnose the runaways if a more suitable set of hard X-ray detectors were installed. In addition very fast instabilities have been observed which appear as fast spikes in the hard X-ray emission.

The decay time of the runaway current is too short to be accounted for by synchrotron losses or by scattering of the runaways from residual plasma ions. It is possible that another mechanism is at work such as the proposed toroidal field ripple scattering.

It would appear that the damaging effects of the runaways could be avoided by properly controlling their position and preventing them from interacting with the vessel walls. The decay time of the current could be reduced if a high density of high Z gas (eg Neon) was introduced into the torus to increase the scattering of the runaways.

ACKNOWLEDGEMENT

It is a pleasure to thank members of the JET team who have contributed to this paper either by providing data or by stimulating discussions.

APPENDIX - SOFT AND HARD X-RAY DETECTORS.

The soft X-rays are observed with horizontal and vertical cameras[19]) almost in a single plane (fig. 13). These contain 100 detectors in total and provide detailed measurements of X-ray emission. Various Be filters may be put in front of the detectors to provide coarse energy resolution and, in addition, a few detectors are shielded by a very thick sheets of stainless steel and are sensitive only to high energy (~MeV) radiation which can penetrate the camera structures.

In addition, a set of toroidal cameras, each with 4 detectors, view the plasma 20-40 cm above the median plane. These have fixed Be filters of 250μm. The location of all of these detectors is shown schematically in fig. 1.

When runaways are present in the plasma it is observed that the relative hard X ray signal intensity in detectors D and B are in the ratio 5:1. Both detectors are shielded from the direct bremmstrahlung radiation from runaway-impurity ion interactions as can be seen in the diagram. It is therefore probable that the observed X-ray hard signals are a consequence of the bremsstrahlung radiation striking the outer plate of a main horizontal port: this then produces secondary radiation which is detected in either the B or D toroidal detectors with relative efficiency determined by the squares of the different distances between the point of impact and the detectors. The square of the ratio of these distances is ~5 in good agreement with the observed values.

In order to make of use of the measured intensities it is necessary to know the absolute detector's efficiency. It is assumed that N bremsstrahlung quanta/sec of energy E strike the port plate of density ρ and thickness t at an angle from the normal χ. For relativistic energies the main interactions of these quanta will be Compton scattering and pair production. For high energy quanta $E >> m_e c^2$ the pair production processes will produce a shower which is predominantly in the forward direction and will not be seen by the detectors. At low E, pair production is unimportant and it would therefore seem that the effects Compton scattering through angles $\theta \sim 90^\circ$ only need be considered.

The Compton scattered flux of gamma rays is

$$\frac{dN_s}{d\Omega} = \frac{N\rho t}{Am_p \cos\chi} \frac{d\sigma_c}{d\Omega}$$

where A is the atomic weight of the port plate atoms and m_p the mass of 1 mu. The Compton polarisation averaged cross-section $d\sigma_c/d\Omega$ is[17])

$$\frac{d\sigma_c}{d\Omega} = \frac{r_o^2}{2}\left(\frac{E_s}{E}\right)^2 \left\{\frac{E}{E_s} + \frac{E_s}{E} - \sin^2\theta\right\}$$

with r_o the classical electron radius. The scattered quanta have energy $E_s = E/(1+(1-\cos\theta)E/m_ec^2)$. For $\theta \sim 90$ and $E >> m_ec^2$, $E_s = m_ec^2$, i.e. 511 keV. If there is an absorber (with transmission T) between the point of scatter and the detector, situated at a distance, d, then the power at the detector is

$$P = \frac{T}{d^2}\frac{pt E_s}{Am_p \cos\chi}\frac{d\sigma_c}{d\Omega}\frac{P_F}{E}$$

where P_F is the power striking the flange. This will produce power in a detector given by

$$P_x = \lambda m_d P/\rho$$

where ρ and m_d are the density and mass of the detector and λ is the main absorption coefficient for Si. The expression for P_x may be then written

$$P_x = \frac{m_d \rho t}{pd^2 Am_p \cos\chi}\left(E_s \lambda T \frac{d\sigma_c}{d\Omega}\right)\frac{P_F}{E} = \varepsilon(E)\frac{P_F}{E}$$

The first term is a constant for a particular detector (9.5×10^{17} for detector D) and the term in brackets depends only on the incident photon energy, E. The efficiency $\varepsilon(E)$ is shown in Fig. 14. The efficiency of detector D may be conveniently written as

$$\varepsilon = 1.4\times10^{-22}\, E_M/(1+0.5\, E_M)^2$$

where E_M is the gamma ray energy in units of MeV.

REFERENCES

1) Wesson, J.A., Gill, R.D., Hugon, M., Schüller, F.C., et al. Nuclear Fusion 29(1989)641.

2) Jarvis, O.N., Sadler, G. and Thompson, J.L. Nuclear Fusion 28(1988)1981.

3) Harris, G.R. JET-R(90)07.

4) Joyer, P. and Martin, G. Controlled Fusion and Plasma Heating 14B(1990)303 (Amsterdam Conference, European Physical Society, Eds. Brifford, G., Nijsen-vis, A. and Schüller, F.C.).

5) Finken, K.H., Watkins, J.G., Rusbuldt, D., Corbell, W.J. et al. Controlled Fusion and Plasma Physics 13B(1989)147. (Venice Conference, European Physical Society, Eds. Segre, S, Knoepfel, H and Sindoni, E.).

6) Bondeson, A., Nuclear Fusion 31(1991)1695.

7) Wesson, J.A., Ward, D.J. and Rosenbluth, M.N., Nuclear Fusion 30(1990)1011.

8) Vanucci, A. and Gill, R.D. Nuclear Fusion 31(1991)1127.

9) Howard, J. and Persson, M. Nuclear Fusion 32(1992)361.

10) Fredrickson, E.D., McGuire, K.M., Bell, M.G., Bush, C.E., et al. Nuclear Fusion 33(1993)141.

11) Ward, D.J., Gill, R.D., Morgan, P.D. and Wesson, J.A.Controlled Fusion and Plasma Heating 12B(1988)330 (Dubrovnik Conference, European Physical Society, Ed. Heijn, J.).

12) Ward, D.J. and Wesson, J.A. Nuclear Fusion 32(1992)1117.

13) Knöpfel, H and Spong, D.A. Nuclear Fusion 19(1979)785.

14) Fussman, G. Nuclear Fusion 19(1979)327

15) Russo, A.J. IAEA Technical Committee Meeting on Avoidance and Control of Tokamak Disruptions, Culham, 1991.

16) Russo, A.J. Nuclear Fusion 31(1991)117

17) Tucker, W.H. Radiation Processes in Astrophysics, The MIT Press, Cambridge, USA(1975).

18) Laurent, L. and Rax, J.M. Europhysics Letters 11(1990)219.

19) Edwards, A.W., Farhbach, H-U., Gill, R.D., Granetz, R. et al. Rev. Sci. Instrum. 57(1986)2142.

20) Gill, R.D. and Edwards A.W. 1992 International Conference on Plasma Physics 16C(1992)355. (Innsbruck Conference, Eds. Freysinger, W. et al).

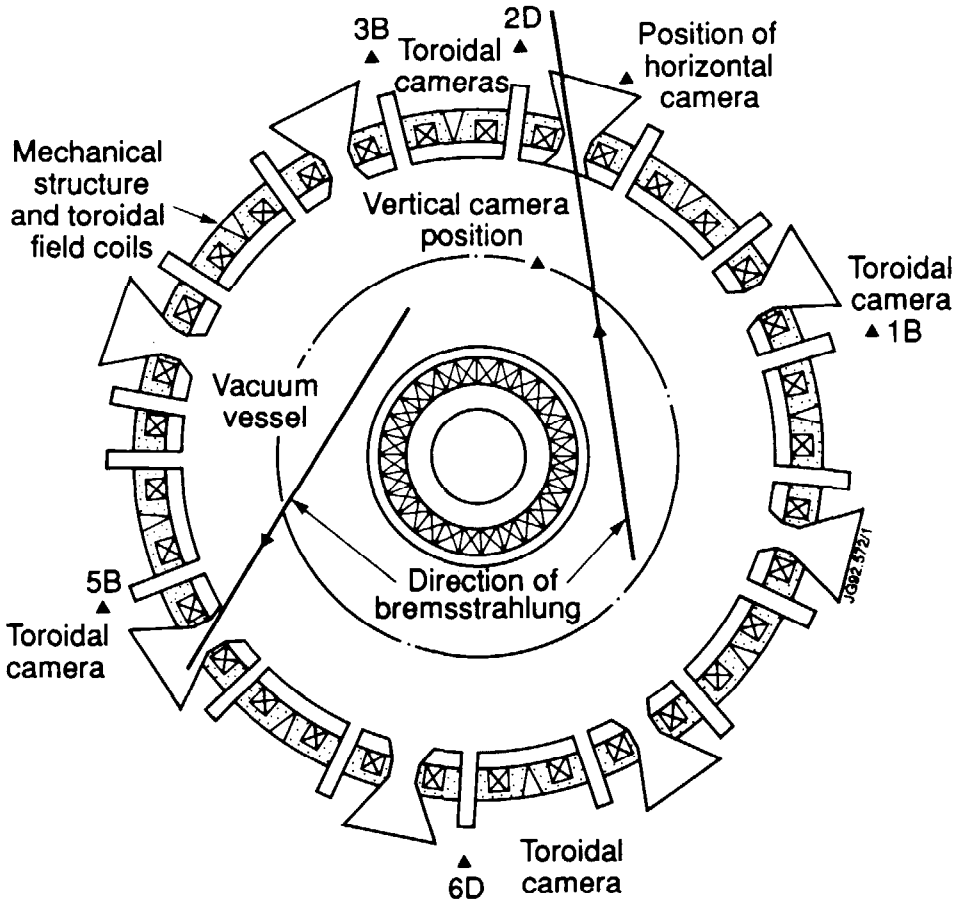

Fig. 1 Plan of JET showing the position of the Si diode detection systems, the coils, ports and mechanical structure. The direction of the current is also shown.

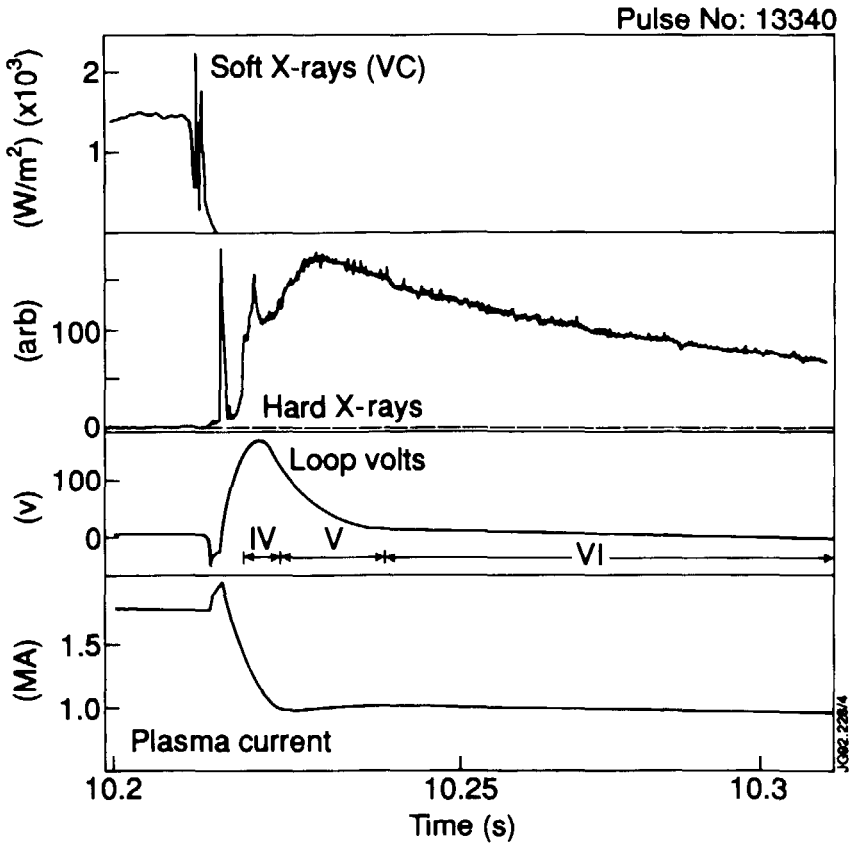
Pulse No: 13340
Soft X-rays (VC)
(W/m^2) (x10^3)
2
1
(arb)
100
0
Hard X-rays
Loop volts
(v)
100
0
IV
V
VI
(MA)
1.5
1.0
Plasma current
10.2
10.25
10.3
Time (s)

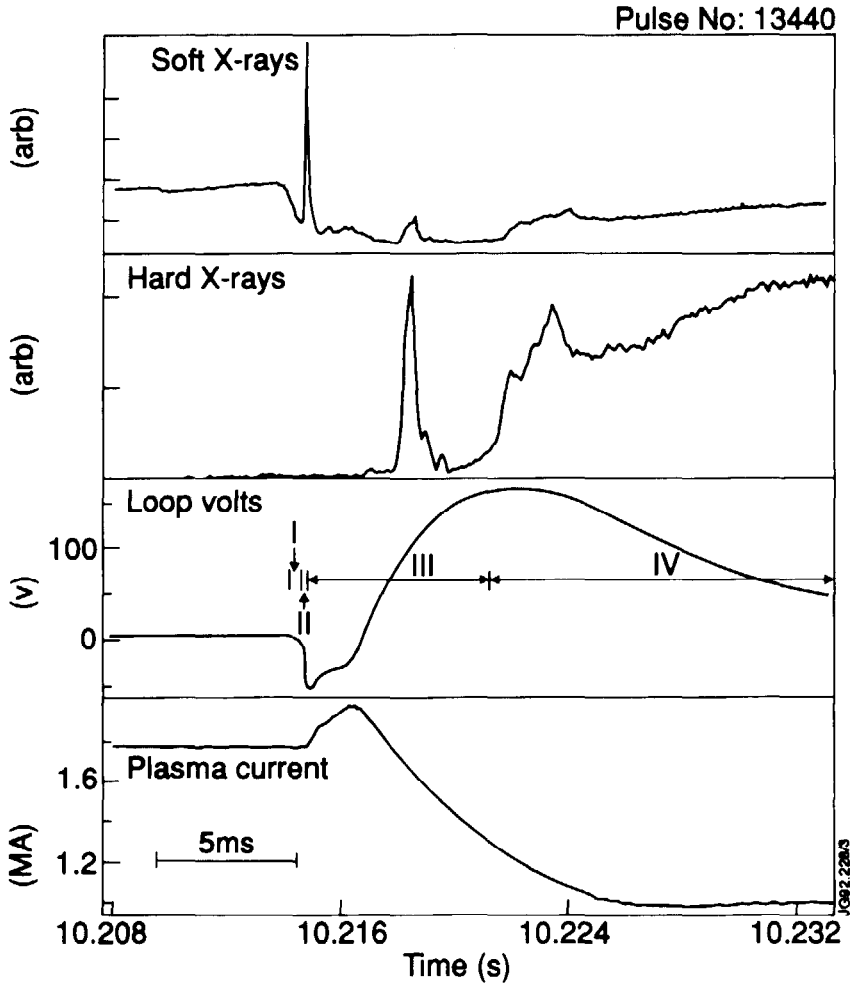
Pulse No: 13440
Soft X-rays
(arb)
Hard X-rays
(arb)
Loop volts
(v)
100
0
I
II
III
IV
1.6
1.2
(MA)
Plasma current
5ms
10.208
10.216
10.224
10.232
Time (s)

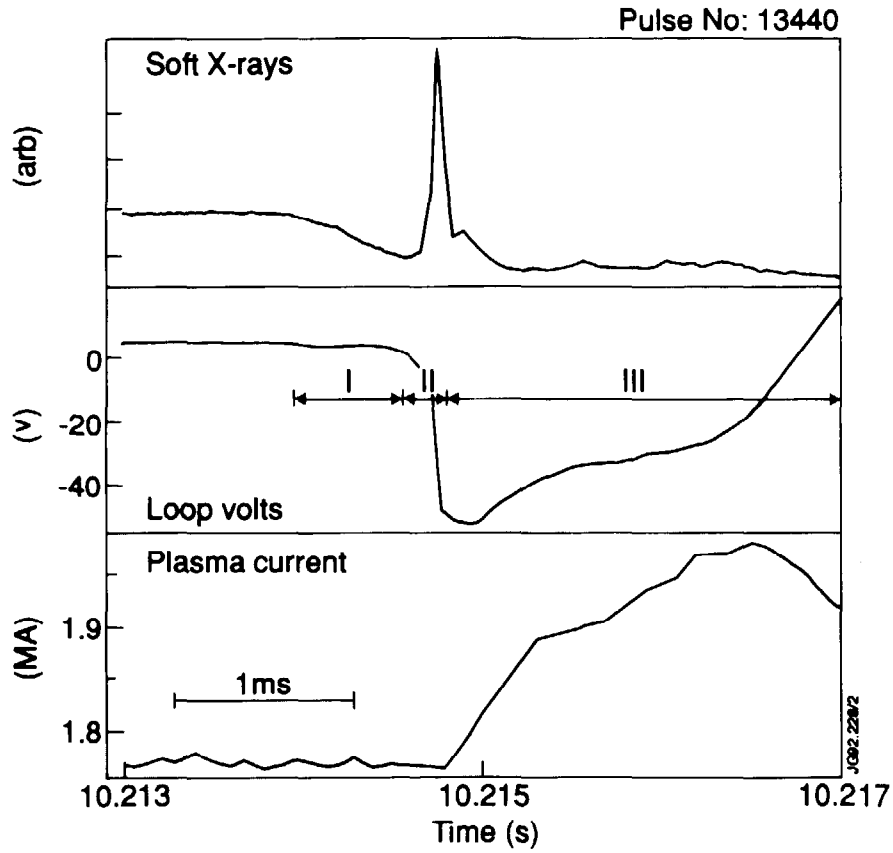

Fig. 2 A plasma disruption is shown which leads to a state with a 1MA runaway current (a) on the slowest timescale the rapid drop in plasma energy content may be seen together with a short negative voltage spike followed by the current decay down to its plateau value of 1MA. (b) On a fastertimescale more detail may be seen on the current and loop voltage traces. The pronounced spike on the soft X-rays may be seen and also the delayed onset of the hard X-rays (c) or the fastest timescale the profile erosion stage I may be seen in relation to the V, I traces.

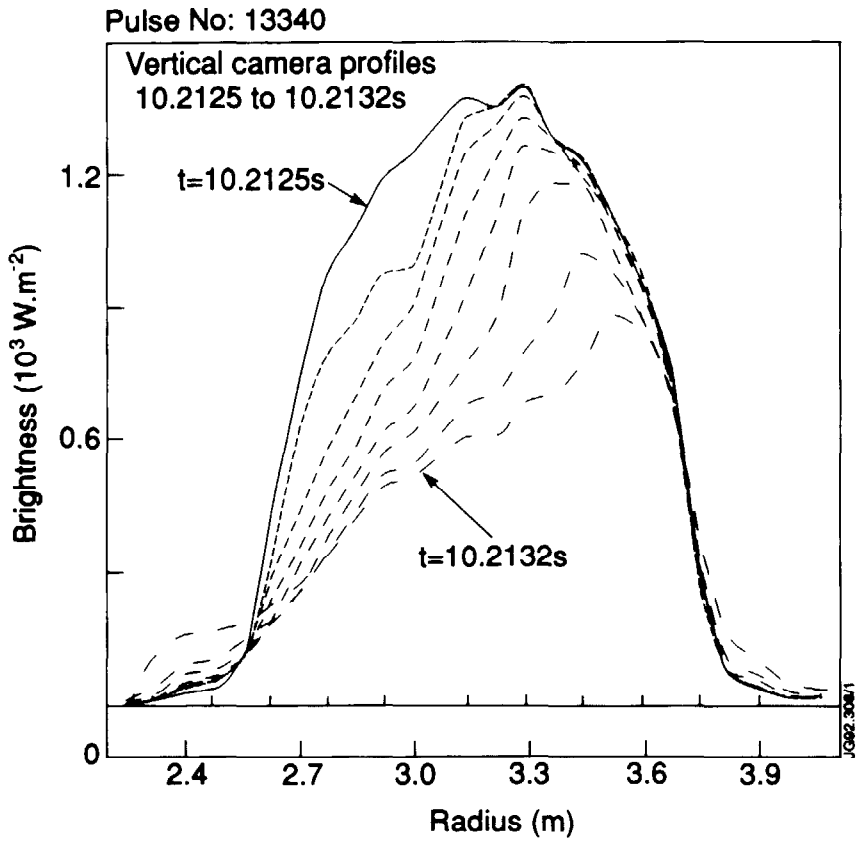

Fig. 3 The profiles of line integrated soft X-ray emission are shown at various times during the profile erosion for the same shot as shown in fig. 2. Initially the erosion affects only a small volume of the plasma at R=2.9m but the volume affected gradually spreads to the whole of the central region. There are 100μsec intervals between successive profiles.

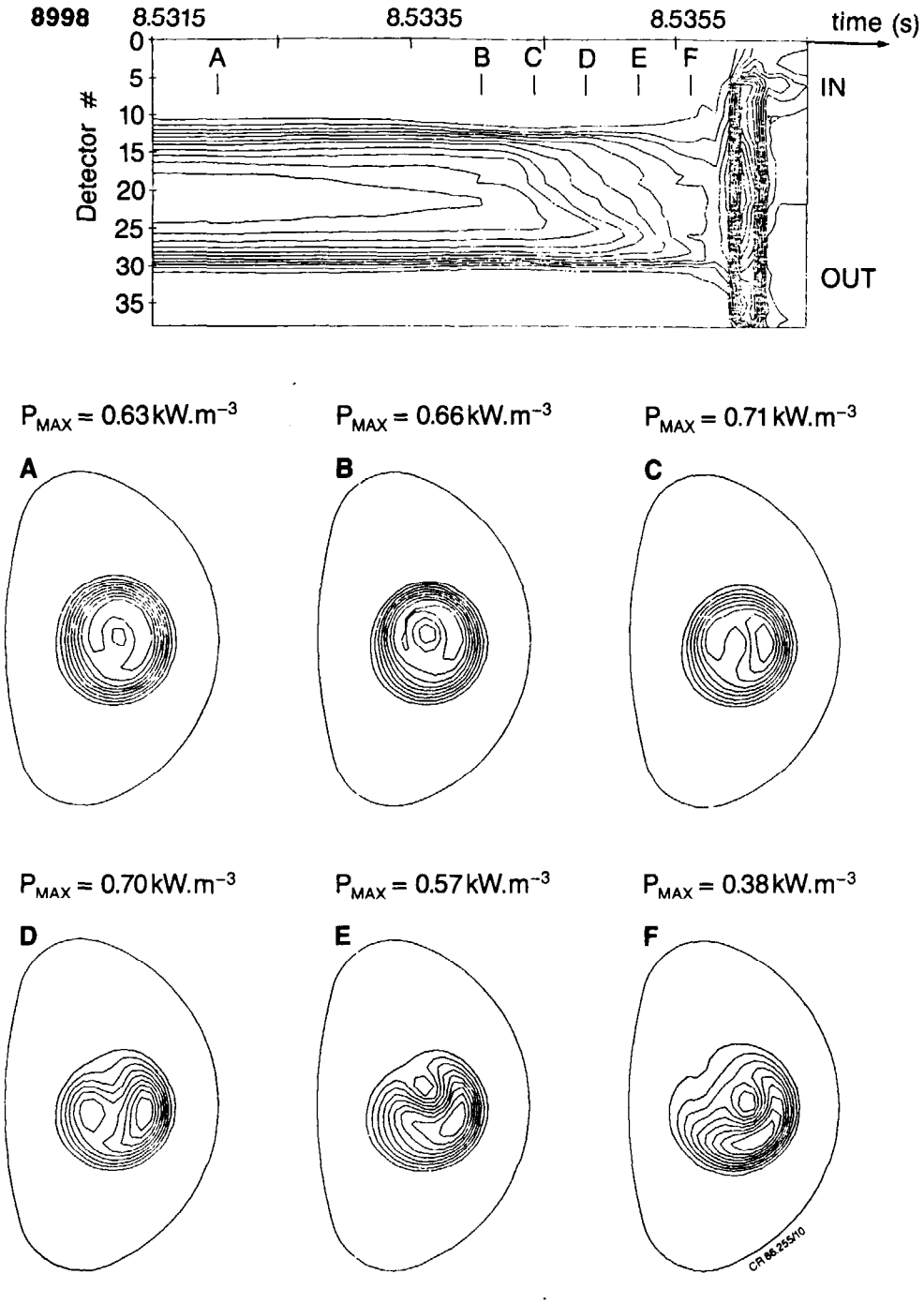

Fig. 4 X-ray emission during the last 5ms before a disruption. The left hand part of the figure shows contours of the line integrated emission versus time, and the tomographically inverted contours at various times are shown on the right. The development of the cold bubble, which has an m=1 character, is clearly seen.

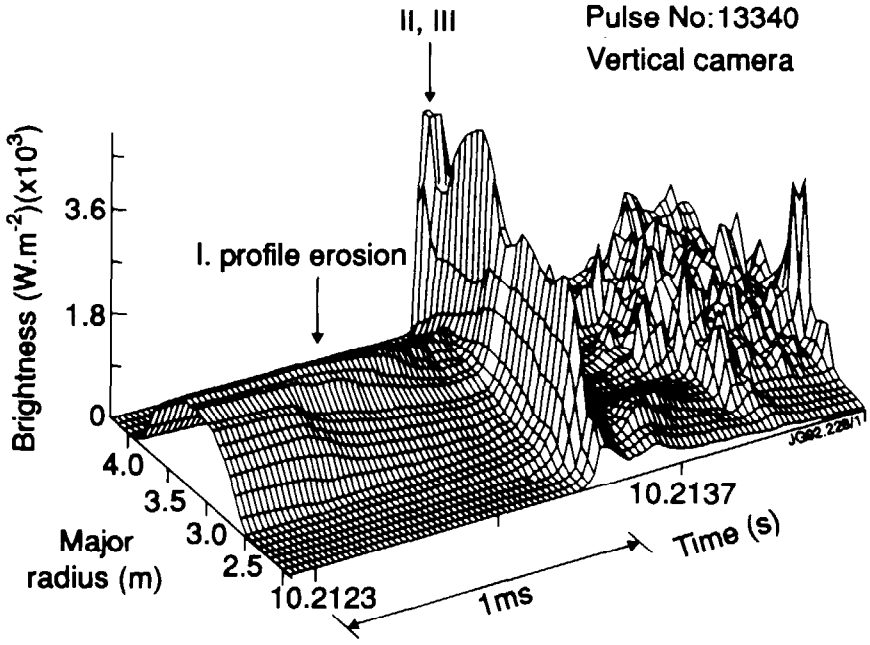

Fig. 5 Plot of X-ray intensity as a function of major radius and time. The profile erosion feature, the front spike and the noisy post disruption emission can be clearly seen.

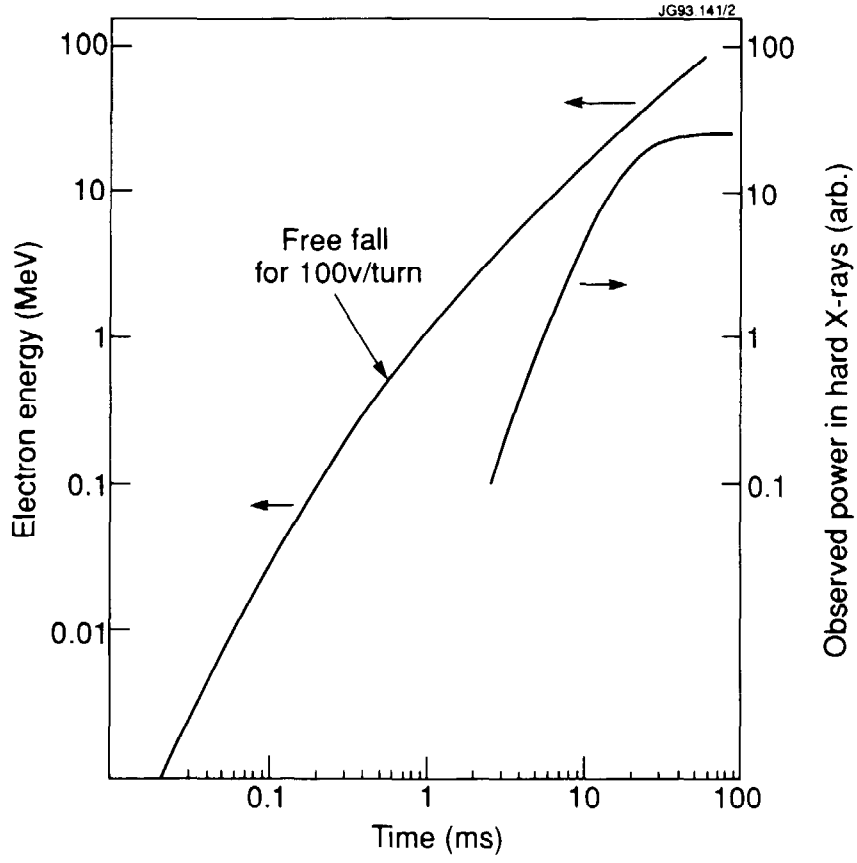

Fig. 6 Runaway energy as function of time with a loop volts of 100v.

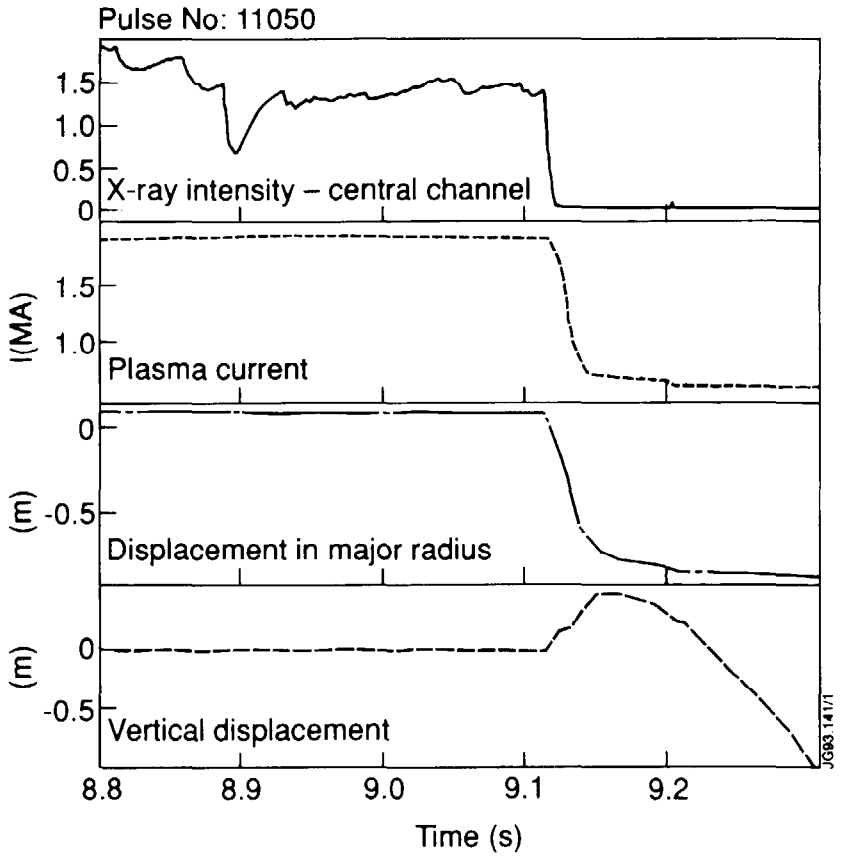

Fig. 7 The plasma position and current are shown. It can be seen that the current channel moves from the plasma centre before disruption to near the inner wall at R=225 cm.

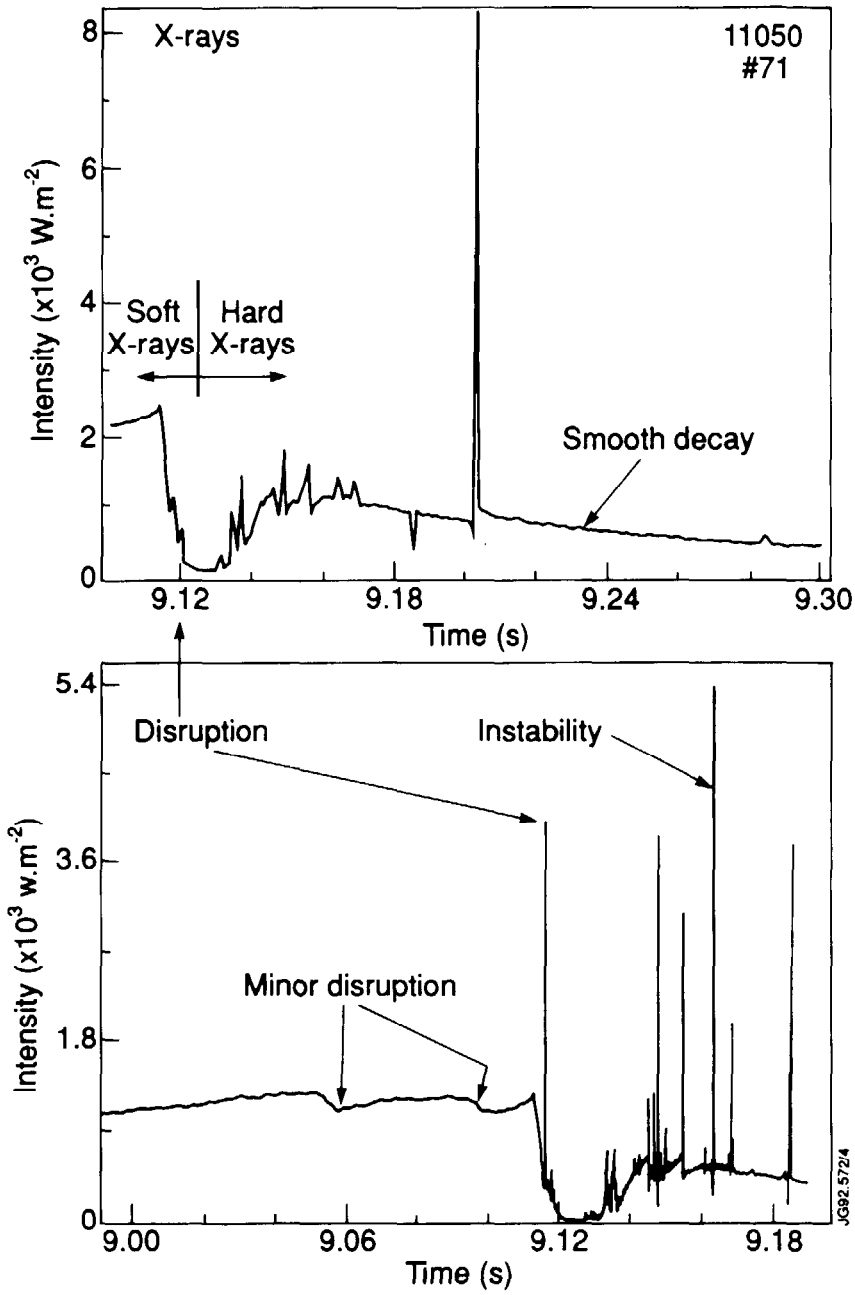

Fig. 8 The X-ray signal after disruption is due to hard radiation and exhibits a build up followed by a smooth decay with both stages punctuated by a series of sharp spikes due to instabilities.

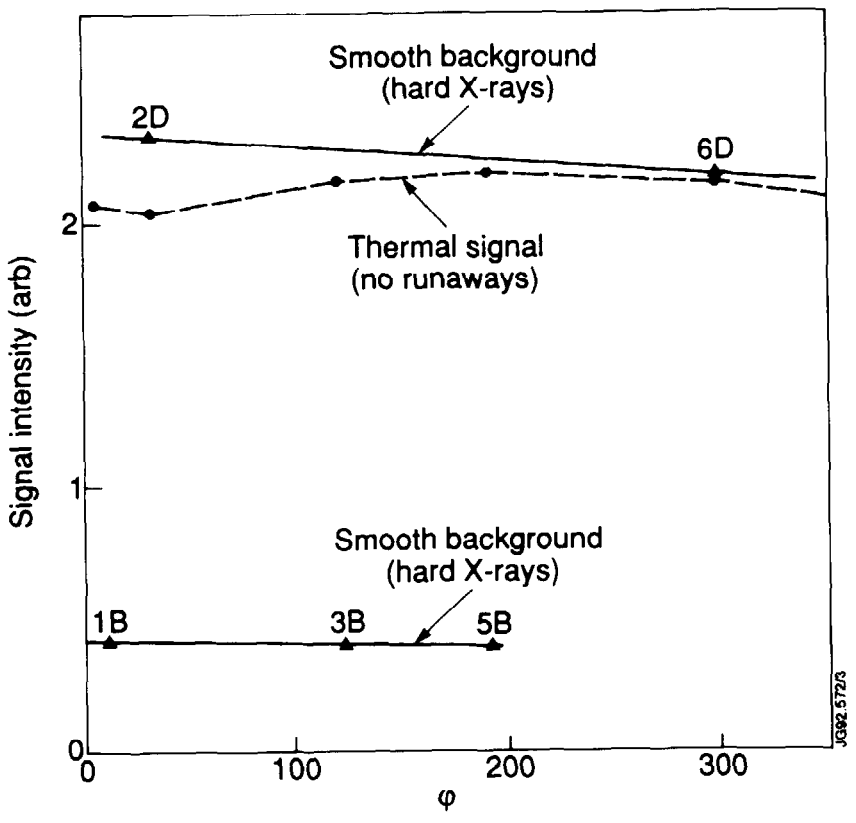

Fig. 9 The toroidal intensity variation is shown for detectors D and B for both the thermal plasma soft X-radiation and the hard X-radiation, post disruption, from the smooth background.

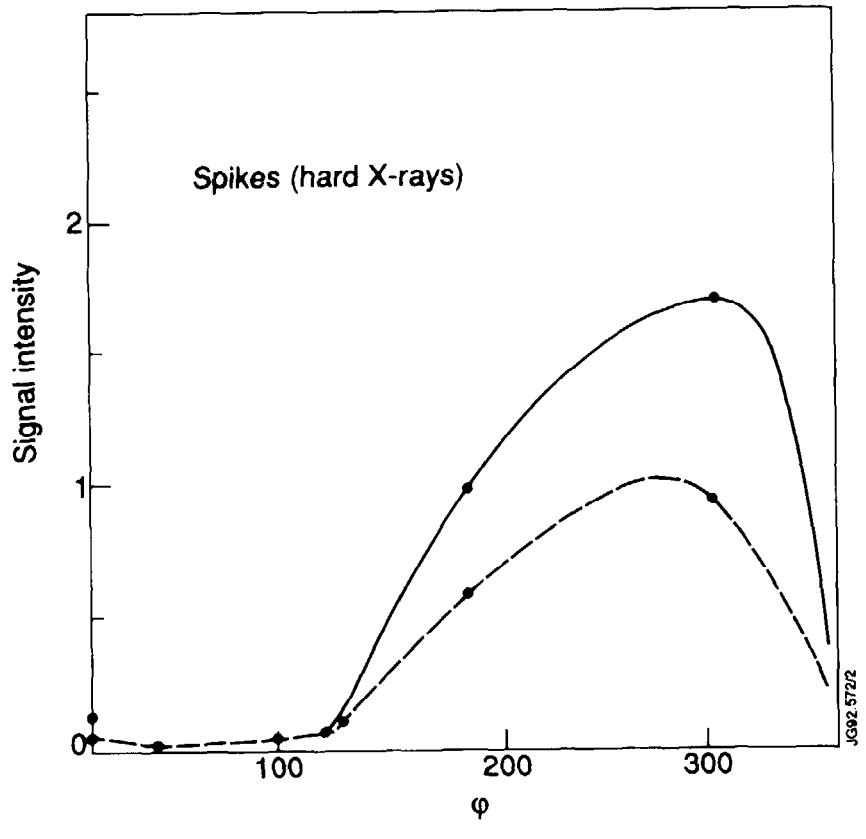

Fig. 10 Toroidal intensity variation of the hard X-ray signals from two of the spikes caused by instabilities.

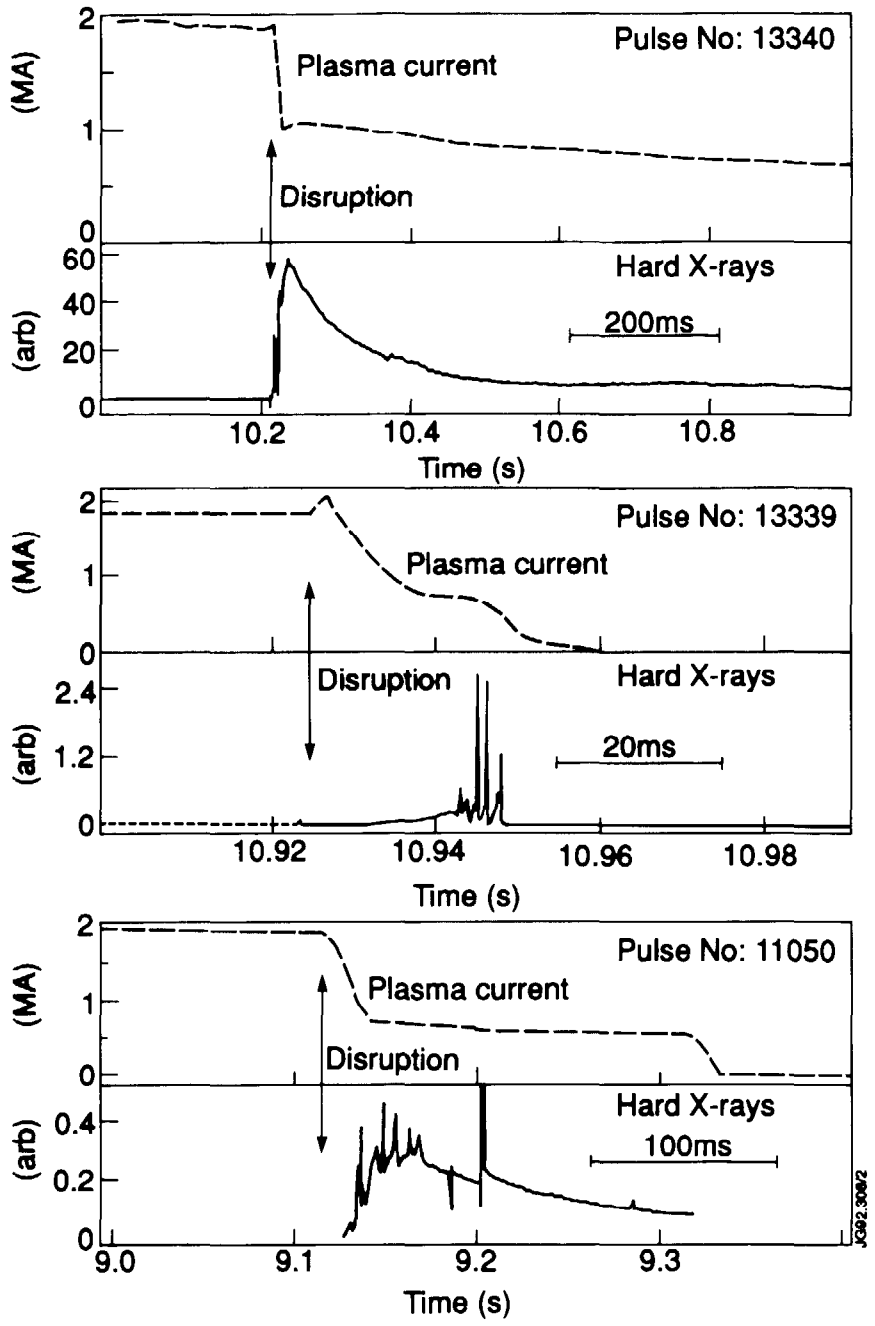

Fig. 11 Three disruptions showing quite different behaviour after the disruptionhas taken place.

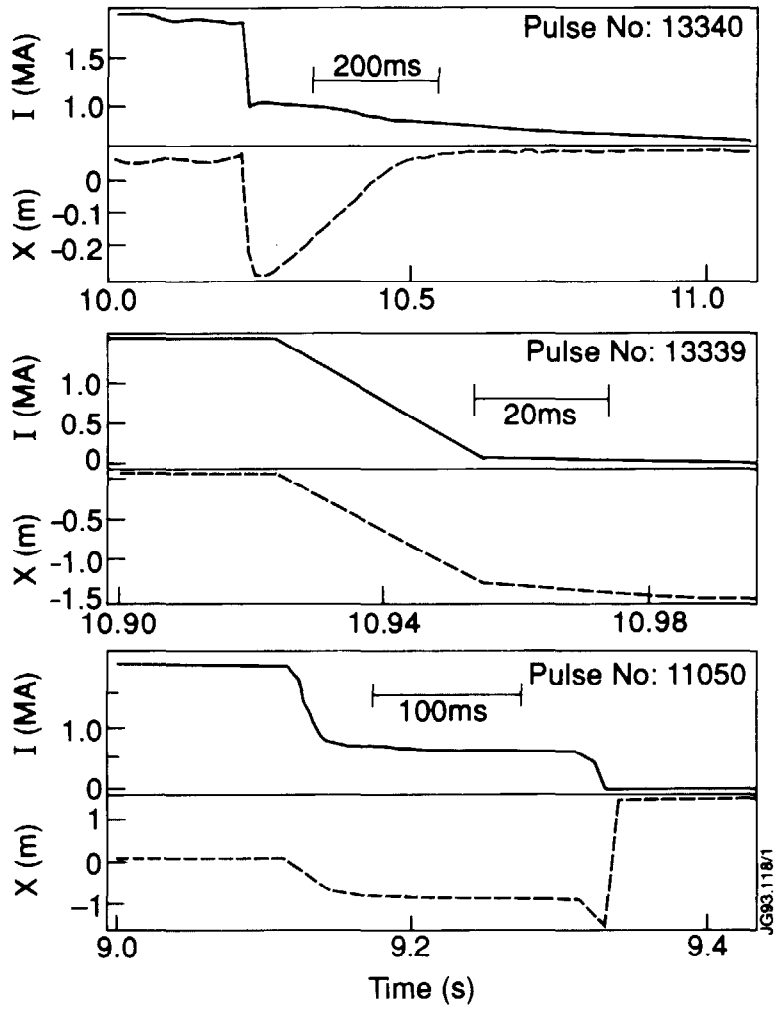

Fig.12 Horizontal displacement of the current channel for the discharges shown in fig. 11.

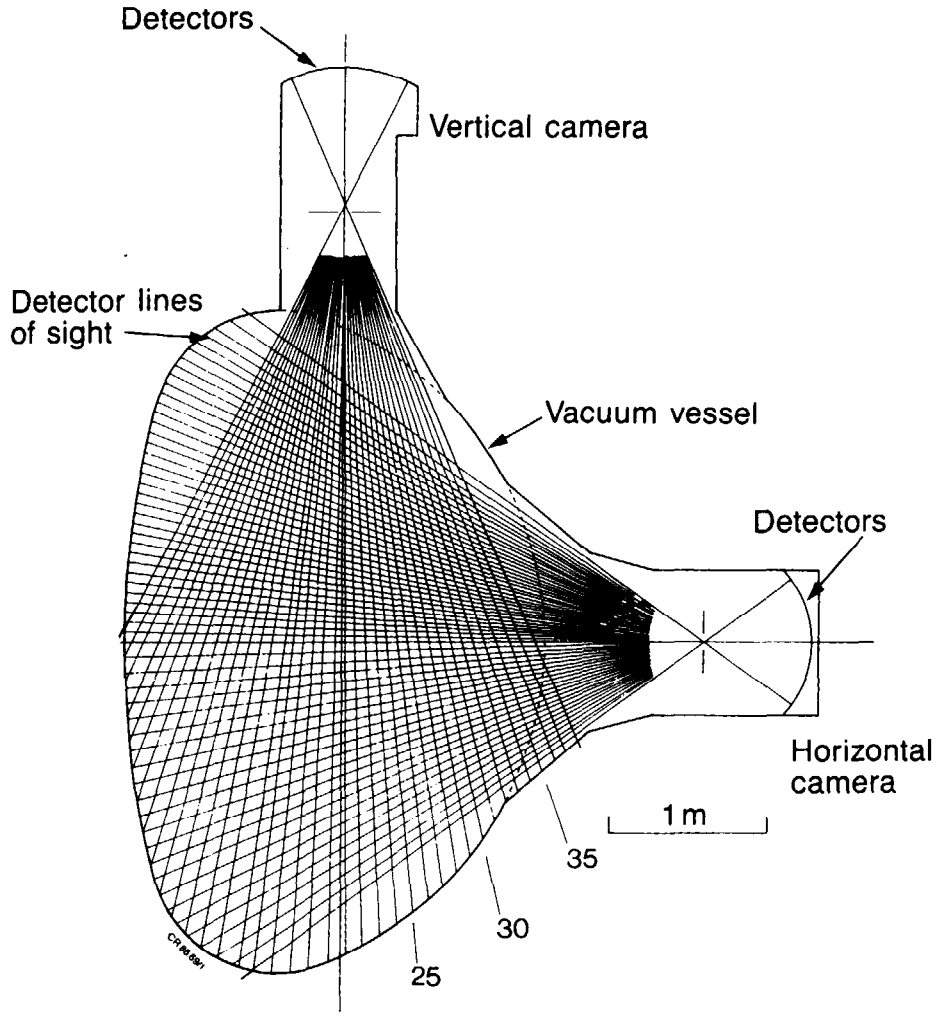

Fig.13 Schematic of the vertical and horizontal soft X-ray cameras.

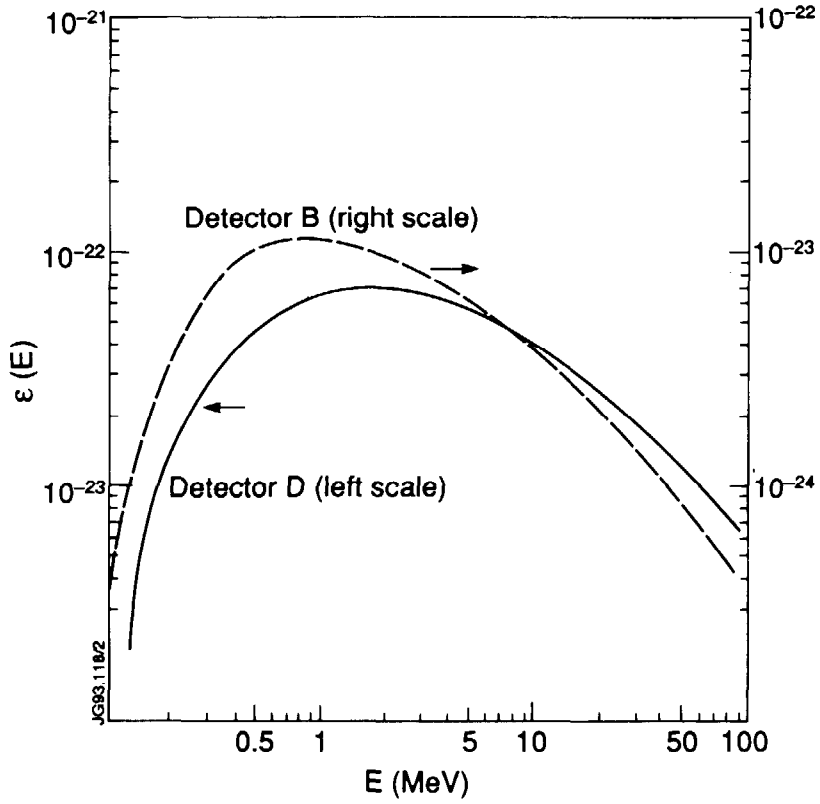

Fig. 14 Detector efficiency as a function of gamma ray energy.